A Rational Biomimetic Approach to Structure Defect Generation in Colloidal Nanocrystals

Lingyan Ruan,[†] Hadi Ramezani-Dakhel,[‡] Chain Lee,[§] Yongjia Li,[†] Xiangfeng Duan,[§,⊥] Hendrik Heinz,[‡] and Yu Huang[†,⊥,*]

[†]Department of Materials Science and Engineering, University of California, Los Angeles, California 90095, United States, [‡]Department of Polymer Engineering, University of Akron, Akron, Ohio 44325, United States, [§]Department of Chemistry, University of California, Los Angeles, California 90095, United States, and [⊥]California NanoSystems Institute, University of California, Los Angeles, California 90095, United States

ABSTRACT Controlling the morphology of nanocrystals (NCs) is of paramount importance for both fundamental studies and practical applications. The morphology of NCs is determined by the seed structure and the following facet growth. While means for directing facet formation in NC growth have been extensively studied, rational strategies for the production of NCs bearing structure defects in seeds have been much less explored. Here, we report mechanistic investigations of high density twin formation induced by specific peptides in platinum (Pt) NC growth, on the basis of which we derive principles that can serve as guidelines for the rational design of molecular surfactants to introduce high yield twinning in noble metal NC syntheses. Two synergistic factors are identified in producing twinned Pt NCs with the peptide: (1) the altered reduction kinetics and crystal growth pathway as a result of the complex formation between the histidine residue on the peptide and Pt ions, and (2) the preferential stabilization of {111} planes upon the formation of twinned seeds. We further apply the discovered principles to the design of small organic molecules bearing similar binding motifs as ligands/surfactants to create single and multiple twinned Pd and Rh NCs. Our studies demonstrate the rich information derived from biomimetic synthesis and the broad applicability of biomimetic principles to NC synthesis for diverse property tailoring.

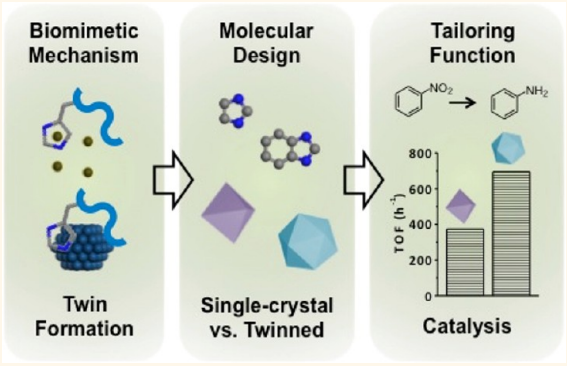

KEYWORDS: noble metal nanocrystals · defect generation · inorganic binding peptides · imidazole complexes · reduction kinetics · attachment growth · catalytic properties

Manipulating the morphology of nanocrystals (NCs) has attracted intense research interests during the past decades due to its fundamental importance and practical applications from catalysis to devices.[1−5] NCs with finely tuned sizes and shapes also lay the foundation of various controlled assembly processes.[6,7] In the classic La Mer model, the formation of NCs usually involves two steps: the initial nucleation of seeds and the following NC growth.[8,9] Following such guidelines, multiple strategies have been developed to manipulate the shapes of NCs, the majority of which focus on tuning the surface energy of facets at the growth stage by choosing appropriate capping agents.[1,8−10] Nevertheless, the final morphology of a NC is determined not only by its displayed facets but also by its initial seed structure, *e.g.*, single-crystal *vs* twinned (single twinned, multiple twinned, *etc.*).[8,9,11] Therefore, controlling the initial seed structure can further enrich available means for the NC morphology control. Oxidative etching has been used to preserve single-crystal seeds and to eliminate twinned seeds for several metal NCs (Ag, Pd, *etc.*);[12,13] while under certain circumstance, twinned seeds are desirable for creating more complex shapes with internal twinned structures (bipyramid, dodecahedron, icosahedron, *etc.*), which have implied influences on NC properties such as catalytic performance, plasmonic response, *etc.*[5,11−14] Nonetheless, fewer strategies are available to rationally generate twinned seeds for metal NCs.[8,9,15−18]

Twinning is an important subject in the field of crystal growth and has been extensively studied in bulk materials or on substrates during vapor deposition for decades.[19−22] More recently, twinning in NCs has started to

* Address correspondence to yhuang@seas.ucla.edu.

Received for review March 28, 2014 and accepted June 12, 2014.

Published online June 12, 2014
10.1021/nn501704k

attract more attention owing to its importance in understanding the shape evolution of NCs and in creation of twinned NCs for desired applications.[11,14,15,23−26] For example, twinned NCs have demonstrated superior performance than their single-crystal counterparts in some catalytic and electrocatalytic reactions.[14] However, twin formation processes in colloidal NCs are still vaguely understood due to complicated growth environment (solvent, surfactant, *etc.*) and different possible growing pathways.[8−18,24,25,27,28] For example, *in situ* transmission electron microscopy (TEM) studies have revealed that both monomer addition and cluster coalescence coexist during platinum (Pt) NC growth, and that structural rearrangement can occur upon coalescence.[27,28] Also, surfactant molecules have been observed to affect the NC nucleation−growth process.[8,9,11,27] While intriguing, so far, the effects of surfactants on NC growth remains a subject requiring further exploration, the understanding of which can enable the design and utilization of surfactant molecules for engineering twinned structures in NCs.[27,28] In this work, we demonstrate a biomimetic approach to reveal the roles of specific peptide surfactant molecules in determining the twin formation in colloidal Pt NCs, and furthermore, we generalize the underlying mechanism to design small molecular surfactants that can promote the formation of single and multiple twinned noble metal NCs.

Nature has demonstrated unrivalled capability of engineering complex material structures through molecular recognition.[29] Inspired by the natural biomineralization process, peptide-directed biomimetic syntheses have appeared as a promising material fabrication method.[30] Various inorganic binding peptides have been exploited and often deliver unique synthetic results.[29−33] For instance, a specific peptide molecule (Thr-Leu-His-Val-Ser-Ser-Tyr, TLHVSSY, named BP7A) has been shown to mediate the growth of single twinned structure in Pt NCs, which had not been reported before.[31] However, information regarding peptide-material interaction upon material formation requires further exploration, which is imperative for the fundamental understanding of organic−inorganic interface as well as the *de novo* material synthetic design.[34−37]

In this study, we aim to investigate the mechanism by which the BP7A peptide introduces twinning in colloidal Pt NCs, and to explore new protocols for artificial manipulation of more complex structures during NC synthesis. Through combined experimental and computational efforts, we have identified two synergetic effects in generating the twinned Pt NCs in the system, *i.e.*, the reduced reduction kinetics through complex formation and the selective stabilization of {111} facet upon twin seed formation. We further demonstrate that the derived principles can be used to design small organic molecular surfactants to generate twinned noble metal NCs, such as palladium (Pd) and rhodium (Rh) NCs, as expected. Twin defects in NCs have recently been reported to be more catalytically active than its single-crystal counterparts.[14,38] To this end, we show that the catalytic activity of twinned Pd NCs is indeed much higher than single-crystal Pd NCs in nitrobenzene hydrogenation reaction. Overall, our studies demonstrate the rich information one could derive from biomimetic synthesis, and the broad applicability of biomimetic principles to engineering colloidal NC structures for many potential applications.

RESULTS AND DISCUSSION

Twinning (or stacking fault) on {111} plane is the most common structural defect for face-centered-cubic (FCC) metals.[21] It can also occur in a single colloidal NC, commonly in the form of planar twin or multiple twins.[8,9,11] Ideally, a single-crystal NC (FCC) under thermodynamic equilibrium would adopt a near cuboctahedral shape (Wulff polyhedron) bounded by the low energy {111} and {100} facets. The occurrence of twins would break this symmetry leading to anisotropic shapes, such as multipods and plates (planar twins), decahedra (5-fold twins), and icosahedra (20-fold twins). The inclusion of twins in a NC can lead to increased internal strain energy, which can be compensated by increased ratio of low energy {111} planes on the surface.[26] Previous studies have shown that single twinned planes in Pt NCs led to a distinct anisotropic multipods morphology, which has also been observed in BP7A mediated Pt NC growth.[31,39] In this study, we examine the effect of various peptides on Pt NC growth by looking at the final morphologies of the Pt NC products, *i.e.*, using the final population of Pt multipods as an indicator of the twin formation introduced by the peptides.

Inorganic binding peptides identified through combinatorial methods are usually diverse in sequences, yet various experimental studies have suggested that certain fragment of a sequence plays a determinant role in the specific binding and functionality.[34−37] To determine which part of BP7A is responsible for the twin formation, we designed a set of BP7A variants through shuffling of residues, truncations into smaller fragments and substitutions of specific residues in the original BP7A, as listed in Table S1 (Supporting Information). We first randomly shuffled BP7A to a new sequence, THSVSLY (termed BP7A-1), to investigate the effect of the specific arrangement of residues in the original BP7A. The BP7A sequence contains several chemical binding motifs, including hydroxyl groups, a phenol group and an imidazole group, all of which have been shown to possess relatively strong binding to metal surfaces.[29,30,32−35,40,41] The imidazole group is located near the N-terminal of the sequence, while the hydroxyl groups are located near the C-terminal of the sequence. Therefore, we truncated BP7A sequence in the middle, yielding TLHV and SSY, to determine the effects of hydroxyl groups and the imidazole group

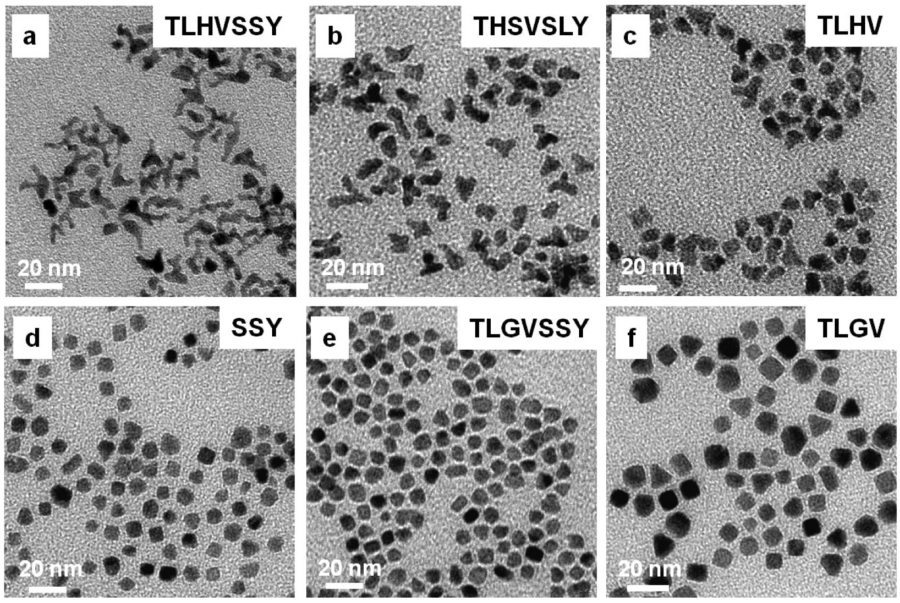

Figure 1. TEM images of Pt NCs synthesized with different BP7A variants. Conditions were kept the same for all reactions, *i.e.*, 1 mM H_2PtCl_6, 1 mM ascorbic acid, 0.08 mM $NaBH_4$, 10 μg/mL peptide, 1 h reaction time. Twinned multipods are the main morphologies produced in reactions (a−c), while single-crystalline cuboctahedra are the main shapes formed in reactions (d−f).

separately. After observing the dominant role of TLHV in the twin formation, we substituted histidine (H) with glycine (G) in both BP7A and TLHV, giving TLGVSSY (termed BP7A-G) and TLGV, to examine the effect of histidine residue. Several more variants, including shuffled sequences TSHVSLY (termed BP7A-2) and TLVH, were designed to further delineate the effects of the residue arrangement and the specific chemical functions of the residues, as presented in Figure S1 (Supporting Information) and discussed in the following section.

We applied the as-designed BP7A variants as surfactant for Pt NC synthesis under the same reaction conditions. As shown in Figure 1, different variants produce quite different NC morphologies. The shuffled variants BP7A-1 (Figure 1b) and BP7A-2 (Figure S1, Supporting Information) produce multipods similar to BP7A (Figure 1a), suggesting the residue arrangement on the sequence is not a determinant factor in twin formation. On the other hand, the two fragments TLHV and SSY produce quite contrastive shapes. TLHV gives multipods morphology similar to that produced by the original BP7A, indicative of twin formation, only with shorter pods (Figure 1c). However, SSY generates near-spherical shape (Figure 1d) that is the characteristic of single-crystal cuboctahedra. We further performed high resolution TEM (HRTEM) characterizations (Figure 2), and confirmed that many of the multipods produced by the shuffled sequence BP7A-1 (Figure 2a−c) and the fragment TLHV (Figure 2d−f) indeed possess twin structures along the pods, similar to the original BP7A peptide,[31] while the near spherical NCs produced by the fragment SSY are single-crystal cuboctahedra (Figure 2g). This suggests that the N-terminal part of the sequence, *i.e.*, TLHV, is responsible for the formation of twin planes. We further shuffled TLHV to TLVH, and observed similar multipods morphology, suggesting that twin formation may be induced by a specific residue on the fragment (Figure S1, Supporting Information). Circular dichroism (CD) measurement also suggests that the peptides are largely random coil in solution without forming specific secondary structures (Figure S2, Supporting Information). Comparing residues on TLHV and SSY, TLHV has an additional imidazole functional group on the histidine residue, which has been suggested to be a strong binder to various metal surfaces.[42] We hence replaced histidine with glycine in both BP7A (BP7A-G, TLGVSSY) and TLHV (TLGV), and observed that instead of multipods, Pt NCs produced by BP7A-G and TLGV display near spherical shapes without twins (Figure 1e−f, Figure 2h,i), confirming the effect of histidine residue in introducing twinning in Pt NCs.

We further investigated the specific role of histidine in introducing twin formation during Pt NC growth. First, TEM images of Pt NCs captured at the beginning stage of the reactions (t = 15 s) show an average seed size of 3.22 nm for the reaction with BP7A (Figure 3b), and an average size of 6.66 nm for the reaction with BP7A-G (Figure 3a), which indicate the histidine containing peptides greatly slow down the NC growth kinetics. The smaller seeds from the reaction with BP7A frequently show twinned structures (~40% frequency under HRTEM, representative HRTEM image in Figure 3b inset), the larger seeds from the reaction with BP7A-G mainly appear single-crystalline (representative HRTEM image in Figure 3a inset), indicating increased twinning

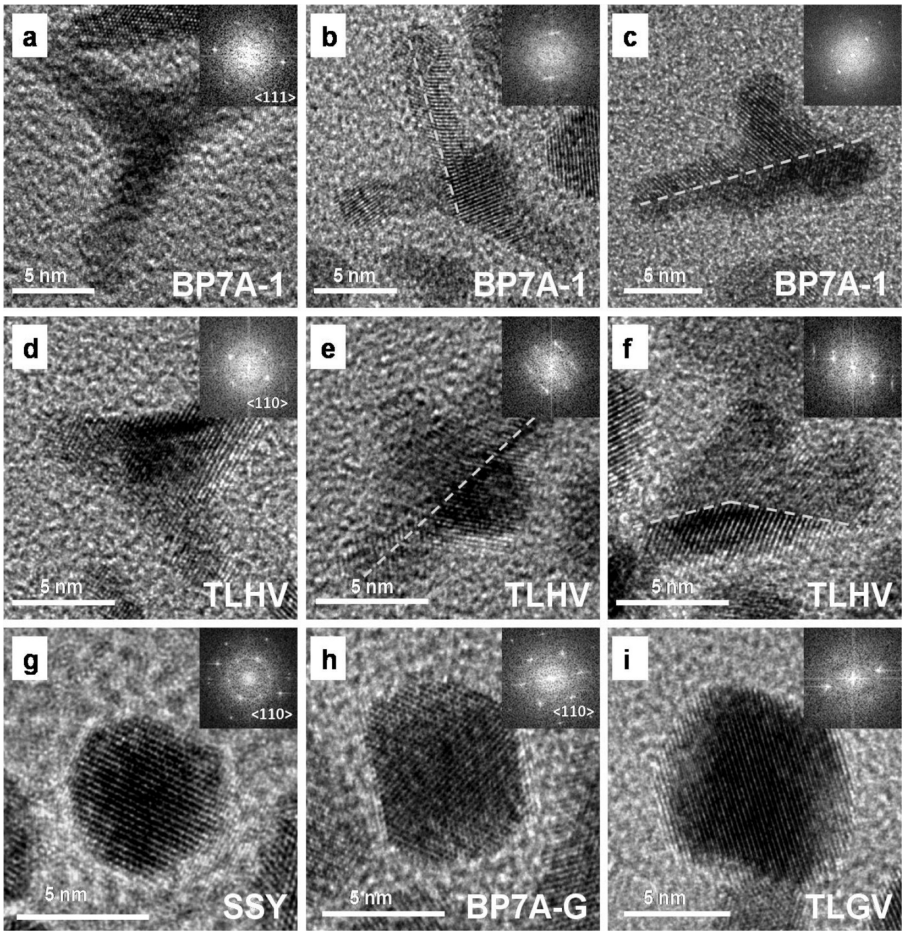

Figure 2. HRTEM images of Pt NCs synthesized with different BP7A variants. (a−c) Structures of Pt NCs produced with THSVSLY. Many multipods show twin planes along the pods, as indicated by dashed lines. (d−f) Structures of Pt NCs produced with TLHV. Similarly, twin planes are also frequently observed along the pods. (g−i) HRTEM images of Pt NCs produced with SSY, TLGVSSY, and TLGV, respectively, showing they are single-crystal cuboctahedral shapes.

event in smaller clusters. Notably, many of the seeds produced by BP7A show nonspherical shapes. We performed tilting HRTEM (Figure 3c,d) and observed the seed bears a twin plane (indicated by the blue dashed line in Figure 3d), which might contribute to its nonspherical shape, confirming increased twinning frequency among the smaller seeds. Interestingly, when BP7A peptide was introduced at a later time frame, *i.e.*, at 30 s after the reaction started, NCs show different growth modes. They first quickly grow into cuboctahedral shapes in the absence of the peptide (Figure 3e), then switch to attachment of small clusters to the corners of the cuboctahedral cores after BP7A was introduced (Figure 3f−h, small clusters are indicated by white arrows), suggesting that the peptide switches NC growth pattern into small cluster attachment.

The formation of smaller clusters in the presence of histidine containing peptide might originate from two aspects: (1) complex formation between the precursor and the peptide leading to slower reduction kinetics; (2) tight binding of the peptide to crystal surface. First, we carried out 1D ^{1}H NMR studies to investigate the interaction between Pt precursor ions and the peptide (Figure 3i).[36] We first tested BP7A peptide with H_2PtCl_6 (Pt(IV)), but did not observe noticeable peak shift (Figure S3, Supporting Information). However, notable peak shift and line broadening was observed in BP7A peptides with K_2PtCl_4 (Pt(II)) (Figure 3i, full spectrum in Figure S4, Supporting Information). Comparison between the spectra of BP7A in the presence and in the absence of K_2PtCl_4 shows that the H(ε) and H(δ) protons of the histidine residue show significant shifts (H(ε) shifts from 8.420 to 8.509 ppm, H(δ) shifts from 7.127 to 7.180 ppm), indicating *strong* interactions between histidine and Pt(II) ion. The two peaks at around 6.7 and 7 ppm could be assigned to protons on the phenol ring of tyrosine (Y), which show less obvious shifts, suggesting much weaker interactions. Line broadening was observed for all protons on histidine and tyrosine, as well as for H(β) of serine (S) (at 3.6−3.8 ppm) and threonine (T) (at 4.2−4.4 ppm), indicating certain degree of interactions between metal ions and hydroxyl groups. Electrospray ionization (ESI) mass spectroscopy (MS) was carried out to further confirm the existence of peptide-Pt(II) complex, where the peptide-Pt and peptide-$PtCl_2$ species were indeed detected in the spectra. (Figure S5, Supporting Information).[43,44] It has been suggested that

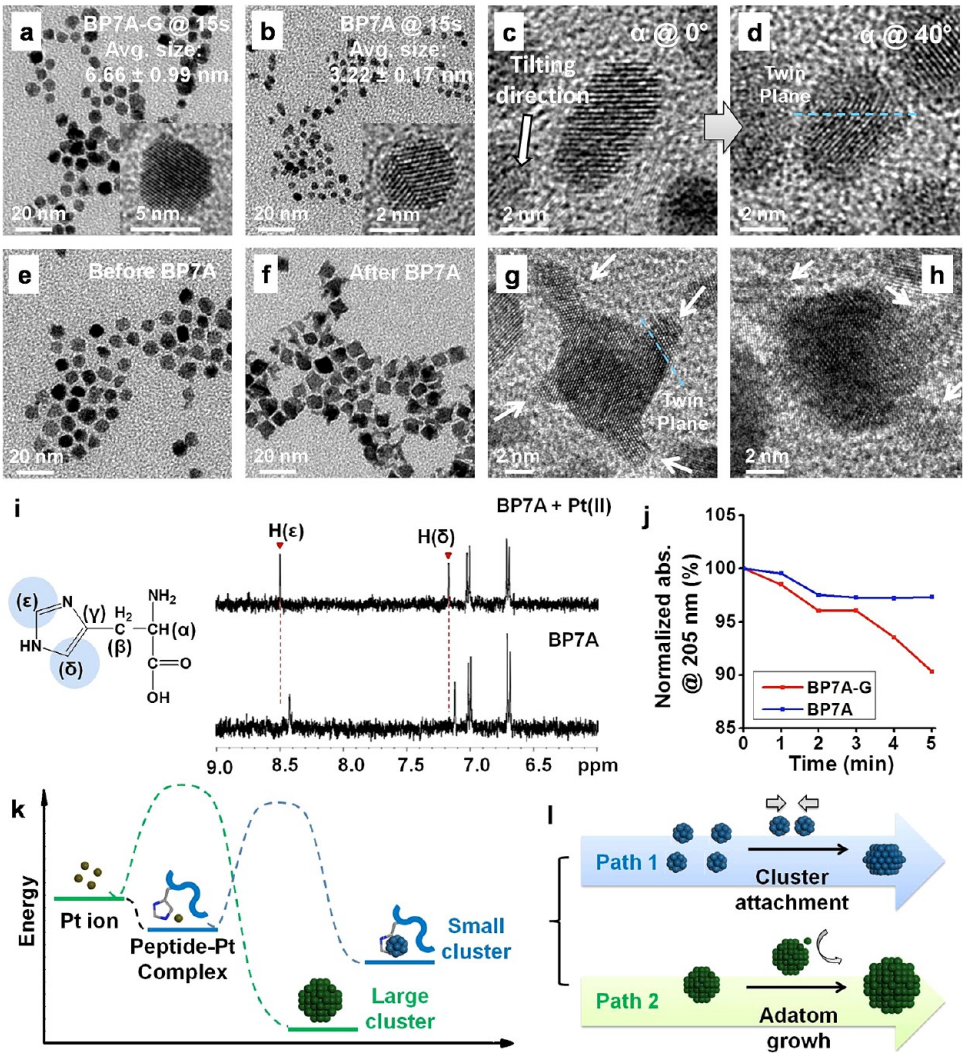

Figure 3. Pt NC growth pathways affected by the BP7A peptide. (a,b) TEM and HRTEM (insets) images of Pt NC seeds obtained at the initial reaction stage (t = 15 s) with BP7A-G (a) and BP7A (b). (c,d) Tilting HRTEM on one of the nonspherical seeds produced by the BP7A peptide, showing it actually bears a twin plane (indicated by the blue dashed line). (e,f) TEM images of Pt NCs before (e) and after (f) introducing BP7A. (g,h) HRTEM images of Pt NCs obtained in (f). The blue dashed line indicates a twin plan observed at the attachment interface. (i) NMR spectra of BP7A peptide interaction with K_2PtCl_4 (5−9 ppm range, full spectrum in Figure S4, Supporting Information). Red arrows and dashed lines indicate the shifts of protons in the histidine residue in the presence of Pt(II). (j) UV−vis spectra of K_2PtCl_4 reduction in the presence of BP7A and BP7A-G peptides (normalized absorption at 205 nm as a function of time). (k) Scheme showing the complex formation between histidine-containing peptides and Pt ions increases the reduction kinetic barrier, leading to small clusters (blue line) instead of large clusters (green line) during the reduction. (l) Scheme showing two possible NC growth pathways: cluster attachment (path 1) and adatom deposition (path 2).

Pt(IV) can undergo multiple-step reductions forming partially reduced intermediate species (such as Pt(II)),[45] and that six-coordinated Pt(IV) is harder to be accessed by ligands than four-coordinated Pt(II).[46] Therefore, it is likely that the peptides form complexes with intermediate Pt(II) species and affect their reduction kinetics.[47] On the contrary to BP7A, BP7A-G shows little shifts/line broadening in the presence of K_2PtCl_4 (Figure S6, Supporting Information), suggesting little interactions between non-histidine-containing peptides and precursor ions.

UV−vis measurement was carried out to study the reduction kinetics of Pt(II) affected by the different peptides (Figure 3j, full spectra in Figure S7, Supporting Information).[48] We monitored the reductions of Pt(II) by sodium borohydride in the presence of BP7A and BP7A-G, respectively. The K_2PtCl_4 solution (aged, containing mainly $PtCl_2(H_2O)_2$) exhibits UV absorption with an absorption coefficient of 1.24×10^4 M^{-1} cm^{-1} at 200 nm, while colloidal Pt NCs exhibit broad and featureless absorption in the spectra that contributes to a higher absorption baseline.[48,49] The reduction of Pt(II) species can therefore be monitored by recording the decrease in the absorption near 200 nm as a function of time (205 nm was chosen in Figure 3j).[48] Upon the addition of sodium borohydride, both reactions show decreased absorption near 200 nm. The reaction with BP7A exhibits slower decrease than that with BP7A-G, indicating the particular role of histidine

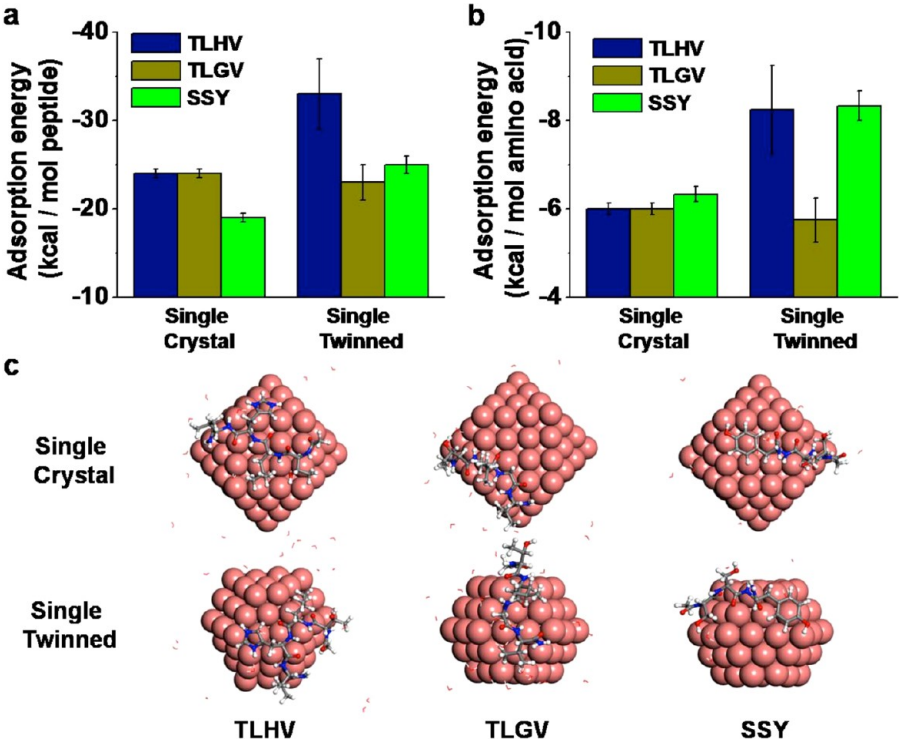

Figure 4. Molecular dynamics simulation of peptide adsorption toward single-crystal and single twinned seed structures. (a) Adsorption energies of peptides TLHV, SSY, and TLGV toward single-crystal and single twinned seeds, respectively. (b) Averaged adsorption energy per amino acid toward single-crystal and single twinned seeds. (c) Representative configurations of peptides on single-crystal and single twinned seeds.

in inhibiting Pt(II) reduction. In addition, the development of an absorption peak at around 220 nm can be attributed to the hydrolysis and formation of $PtCl(OH)(H_2O)_2^{2-}$ species.[48] With BP7A, this peak barely appears compared to the reaction with BP7-G, indicating the suppression of the hydrolysis process which could be due to the strong binding of the peptide to the intermediate species. Also, the development of broad adsorption toward visible light region indicates the formation of colloidal Pt NCs. The reaction with BP7A shows little development of such adsorption (Figure S7, Supporting Information), indicating much slower crystal nucleation and growth in the presence of BP7A. The slower growth rate could originate from the tight binding and confinement of histidine-containing peptide to NC surfaces.[41,50]

Thus far, evidence conjointly supports the following scheme (Figure 3k,l). The complex formation between Pt ions and the BP7A peptide, particularly with the histidine residue, produces an extra kinetic barrier that slows down the reduction kinetics, leading to the formation of smaller seeds observed in previous experiments (Figure 3b). Together with the tight binding of peptides to NC surface, clusters are anticipated to stay small for a prolonged time (blue line in Figure 3k). As a result, cluster attachment event is likely to be significantly enhanced within the system due to the higher surface energy and higher mobility of small clusters (path 1 in Figure 3l).[27] On the contrast, in control experiments with nonhistidine-containing peptides, large clusters quickly form from faster reaction (green line in Figure 3k), which usually prefer to undergo the adatom addition crystal growth (path 2 in Figure 3l).[27] Both growth scenarios have been previously observed *in situ* for Pt NC growth.[27,28]

In the attachment growth, crystallographic matched or mismatched attachments can occur.[24] Structural rearrangement and interface elimination can result in single-crystal or twinned structures, with the former more thermodynamically favored.[24] The high frequency of twinning in Pt NCs observed in our system indicate specific stabilization of twin structures by the histidine-containing peptides. To understand molecular details of the possible stabilization mechanism, we carried out molecular dynamics simulation of peptide adsorption on twinned *versus* single-crystal structures using the CHARMM-METAL force field (Figure 4).[41] The utility of the CHARMM-METAL force field in understanding molecular recognition and shape-dependent adsorption preferences has been noticed earlier.[51−54] Since we mainly observed single twinned planes in Pt NCs, we used a single twinned seed to represent initially formed twinned cluster and a cuboctahedron seed to represent initially formed single-crystal cluster.[31] Both single twinned and single-crystal seeds remain stable during the course of simulation and no reconstruction occurs at room temperature in aqueous solution. To explore the roles of different fragments in the BP7A

peptide and the specific role of histidine, fragments TLHV, SSY, and TLGV were analyzed. In order to minimize the effect of different peptide length, the adsorption energy was averaged over the number of residues on each fragment. As shown in Figure 4a,b, TLHV shows larger adsorption energy (more negative) toward the single twinned seed than the cuboctahedron seed (−33 *vs* −24 kcal/mol peptide, −8.25 *vs* −6 kcal/mol residue), which is consistent with the experimental observation that the population of twinned seeds increases with the stabilization of TLHV (Figure 3b). In contrast, TLGV slightly favors the cuboctahedron seed (−24 *vs* −23 kcal/mol peptide, −6 *vs* −5.75 kcal/mol residue), which is also consistent with the experimental result that TLGV produces single-crystal NCs (Figure 3a). Interestingly, SSY shows larger adsorption energy toward the single twinned seed than the cuboctahedron seed (−25 *vs* −19 kcal/mol peptide, −8.33 *vs* −6 kcal/mol residue), indicating it also has certain degree of stabilization toward twinned structure. However, it produces single-crystal NCs in the experiment (Figure 1d). This can be attributed to the weaker interaction between SSY and Pt ions, supported by little NMR peak shift observed for the phenol protons (Figures S3, S4, S6, Supporting Information). Therefore, we suggest it is the synergetic effects, *i.e.*, the strong interaction between histidine and Pt ions and the preferential stabilization of {111} facets, that contribute to the formation of twinned seeds in Pt NCs. While SSY cannot generate twin seeds, it can stabilize them once generated. This can explain the experimental observation that the whole peptide sequence BP7A (TLHVSSY) produces longer pods than the fragment TLHV (Figure 1a,c), which suggests that SSY promotes the continual growth of pods along twin planes. With this hypothesis, we introduced SSY into reactions with TLHV, and did observe the promotion of pod growth in Pt multipods, with higher SSY concentration leading to longer pods (Figure S8, Supporting Information).

It is quite interesting that both TLHV and SSY can stabilize twinned seeds. Configurations of TLHV and SSY were examined to study the molecular origin of their stabilization effect (Figure 4c). Both TLHV and SSY have aromatic rings on their side chain, showing strong adsorption toward {111} planes of FCC metals according to soft epitaxial and geometric matching.[51,52] As shown in Figure 4c, both the imidazole ring of histidine and the phenol ring of tyrosine lie on {111} planes of the single twinned seeds matching the hexagonal lattice pattern. For FCC metals, twinning occurs on {111} planes, which could break the symmetry and increase the fraction of {111} facets on exposed surface.[26] From the molecular models, we note a major difference between twinned and single-crystal seeds in the bounded {111}/{100} facet ratio (twinned seed: 57/43; single-crystal seed: 37/63). In the presence of the motif that preferentially binds to {111} planes, twin structures may thus be favored over single-crystal seeds. This is also manifested in the root-mean-square displacement (RMSD) calculation of histidine residue generated in simulation, which shows a much smaller value on single twinned seeds when compared to cuboctahedral seeds, indicating tighter binding of the histidine residue on the surface of the single twinned seed (Figure S9, Supporting Information).

To conclude, we have carried out detailed mechanistic studies on the twin formation in Pt NCs mediated by the BP7A peptide, which suggest two necessary conditions for the formation of twinned structures: (1) the decelerated reduction kinetics and the altered crystal growth pathway through the strong interaction between the histidine residue and Pt ions, and (2) the preferential stabilization of {111} planes, which can lead to the favorable stabilization of twinned seeds. We further applied our mechanistic understanding on biomimetic specific binding to the rational selection and design of small capping molecules for the synthesis of twinned structures of noble metals other than Pt, *i.e.*, Pd and Rh. We started with a histidine analogous small molecule imidazole and further chose benzimidazole, which bears an additional benzene ring. A modified polyol reduction method to synthesize single-crystal cuboctahedral Pd and Rh NCs was used,[55] wherein imidazole or benzimidazole were introduced as additives. Without the introduction of the small molecules, resultant Pd NCs show slightly truncated octahedral shape (Figure 5b,c) and Rh NCs display truncated cube shape (Figure 5i,j), which are all single-crystal in nature. When imidazole was introduced, Pd NCs show increased population of icosahedra (Figure 5d,e, about 50% icosahedra). For Rh NCs, twinned structures in a mixture of single twins and multiple twins also increase in percentage, with single twins prevailing over multiple twins (Figure 5k,l). The HRTEM image in Figure 5l shows a typical single twinned Rh NC, and more structural characterizations are shown in Figure S10 (Supporting Information). Following the second derived principle that stabilizing {111} facet can favor the stabilization and growth of twin structures of FCC metal NCs, we tested the effect of benzimidazole, which is expected to have enhanced adsorption toward {111} facets as a result of its additional benzene ring.[35,51,52,56] Supporting our hypothesis, both Pd and Rh NCs synthesized with benzimidazole show further increased yields in multiple twinned NCs. For Pd NCs, icosahedra appear as the dominant final shape (Figure 5f,g). For Rh NCs, multiple twins appear as the preferred structure, exceeding the population of single twinned ones (Figure 5m,n, Figure S11, Supporting Information). The increment of multiple twinned NCs can be attributed to the stronger adsorption of benzimidazole molecules to {111} facets, compensating the strain energy produced by the twin formation.[8,11,22,26] The formation of different twinned structures, *i.e.*, single twin, 5-fold twin (dodecahedron) or 20-fold twin (icosahedra) likely involves more factors. Metal ion-ligand complex

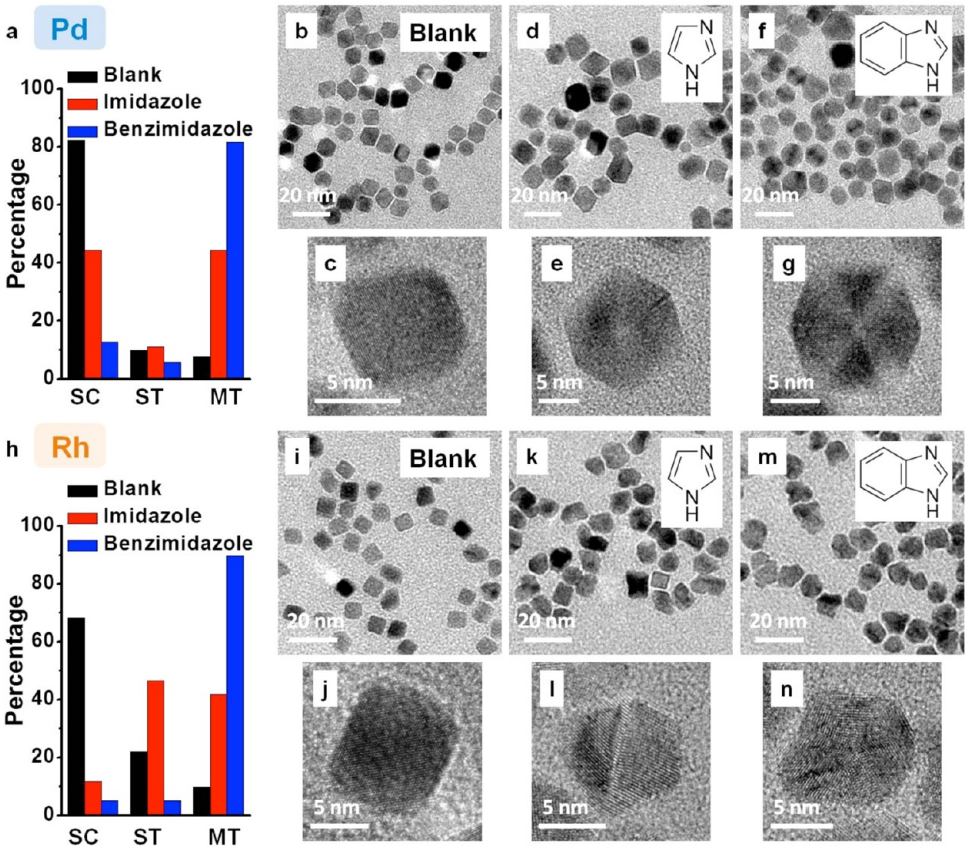

Figure 5. Pd and Rh NCs synthesized with imidazole and benzimidazole. Conditions were kept the same for all reactions, except for the use of imidazole and benzimidazole as additives. (a) Percentage of single-crystal (SC), single twinned (ST) and multiple twinned (MT) Pd NCs synthesized in (b,d,f). (b−g) TEM/HRTEM images of Pd NCs synthesized with no additive (blank), with imidazole, and with benzimidazole, respectively. (h) Percentage of single-crystal (SC), single twinned (ST) and multiple twinned (MT) Rh NCs synthesized in (i,k,m). (i−n) TEM/HRTEM images of Rh NCs synthesized with no additive (blank), with imidazole, and with benzimidazole, respectively.

coordination, reduction kinetics, growth pathway, twin formation energy, and surface energy can all play a role in more selective NC growth.[8,9,45,48,49,56] Our demonstration here provides the ground for further exploration of fundamental understandings of twin formation and of synthetic approaches that could rationalize twin formation through the design of appropriate capping molecules.

Engineering NCs with twin structures can be beneficial for catalytic and electrocatalytic performances.[14,38] As a demonstration, we studied the hydrogenation of nitrobenzene catalyzed by Pd NCs, an effective hydrogenation catalyst.[57] We compared catalytic activities between single-crystal and multiple twinned Pd NCs (Table 1). In a typical reaction, nitrobenzene is converted into aniline in hydrogen gas by Pd NCs.[57] Both single-crystal and multiple twinned Pd NCs show effective conversion of nitrobenzene (Figure S12, Supporting Information), with the twinned NCs displaying a much faster conversion rate than the single-crystal ones. For example, nearly 100% conversion was achieved in 105 min for twinned NCs, while it took 150 min to reach 100% conversion for single-crystal NCs. The catalytic activity was further normalized to the intrinsic turnover frequency (TOF, defined as the nitrobenzene conversion per surface metal atom per second). The TOFs of single-crystal and multiple twinned NCs were calculated to be 373 h^{-1} and 694 h^{-1}, respectively, indicating improved catalytic activity in the presence of twin structures. The enhanced performance can be ascribed to the improved hydrogen adsorption capability of multiple twinned NCs and the more active surface atoms due to strain.[14,58,59] The large TOF difference clearly demonstrates that twinning in NCs can be an effective strategy to improve the catalytic performance. Moreover, as revealed by TEM characterizations, NCs maintain their morphology after catalytic reactions (Figure S13, Supporting Information).

TABLE 1. Catalytic Results of Nitrobenzene Hydrogenation by Pd NCs

Pd NCs	mole of surface atoms	conversion at 60 min (%)	TOF (h^{-1})
single-crystal	1.345×10^{-6}	41.82	373
multiple-twinned	1.21×10^{-6}	70.02	694

CONCLUSION

In summary, we have studied the mechanism of twin formation in Pt NC growth under the influence of a specific Pt binding peptide BP7A and have discovered

two key roles played by the peptide. Most importantly, the histidine residue in BP7A is found to interact strongly and form complexes with Pt ions, which decelerates the reduction kinetics of Pt precursors and leads to increased Pt NC growth through cluster attachment. At the same time, the histidine residue shows specific stabilization toward twinned seeds through the strong adsorption and stabilization of {111} planes. Interestingly, the tyrosine residue, showing similar stabilization toward twinned seeds due to its affinity to {111} planes, cannot produce twinned Pt NCs due to the lack of ability to generate twin seeds through decelerating reaction kinetics. We have applied our discovered principles to design small organic molecules for Pd and Rh NC synthesis and obtained anticipated twinned structures. We have further demonstrated the twinned Pd NCs show much improved catalytic activity in the hydrogenation of nitrobenzene when compared with single-crystal NCs. Our studies demonstrate the mechanistic understanding and the broad applicability of biomimetic principles, which provides a potential platform for further exploration of rational biomimetic design and engineering of nanoscale features.

METHODS

Chemicals. Chloroplatinic acid hydrate ($H_2PtCl_6 \cdot xH_2O$, Sigma), potassium tetrachloroplatinate (K_2PtCl_4, Sigma), sodium tetrachloropalladate (Na_2PdCl_4, Sigma), sodium hexachlororhodate (Na_3RhCl_6, Sigma), sodium borohydride ($NaBH_4$, Sigma), ascorbic acid ($C_6H_8O_6$, Sigma), ethylene glycol ($C_2H_6O_2$, Sigma), polyvinylpyrrolidone (PVP, average mol wt: 55 000, Sigma), imidazole ($C_3H_4N_2$, Sigma), benzimidazole ($C_7H_6N_2$, Sigma). All chemicals were applied as received without further purification.

Peptide Synthesis. Peptides were synthesized by fmoc solid phase peptide synthesis technique using a CS 336X synthesizer (C S Bio).[40] The N- and C-terminals of all peptides were acylated and amidated, respectively, to reduce interfering electrostatic interactions. The as-synthesized peptides were purified on a Beckman–Coulter Gold high performance liquid chromatography (HPLC) and characterized on a Shimadzu 2010 EV liquid chromatography mass spectrometer (LC–MS) before usage.

NC Synthesis. Pt NCs were synthesized in aqueous condition at room temperature using peptides as surfactants. In a typical synthesis, H_2PtCl_6 solution (10 mM), peptide solution (1 mg/mL) and H_2O were mixed in a glass vial to desired concentrations. $NaBH_4$ solution (50 mM) and ascorbic acid solution (50 mM) were freshly prepared. The ascorbic acid solution was first introduced into the glass vial, followed by the injection of $NaBH_4$ solution. The final concentrations were 1 mM for H_2PtCl_6, 1 mM for ascorbic acid, and 0.08 mM for $NaBH_4$, respectively. $NaBH_4$ initiates the nucleation process; however, it diminishes quickly after reacting with water. Ascorbic acid can then continue to reduce the residual Pt ion precursor to produce Pt atoms. The Pt NCs were allowed to grow 1 h before characterization. Pd and Rh NCs were synthesized employing the polyol reaction using PVP and small molecules (imidazole/benzimidazole) as surfactants. Ethylene glycol was used as the solvent and reducing agent. In a typical synthesis, PVP and small molecules were dissolved in EG to desired concentrations and heated to 160 °C in an oil bath. Then, Na_2PdCl_4 or Na_3RhCl_6 solutions were introduced dropwise (0.6 mL in 3 min). The final concentrations were 50 mM for PVP, 15 mM for Na_2PdCl_4 or Na_3RhCl_6 and 10 mM for small molecules, respectively. The NCs were allowed to grow 1 h before collection and characterization.

Characterization. NC morphologies were characterized on a FEI CM120 TEM operated at 120 kV and a FEI TITAN STEM operated at 300 kV. FFT (fast Fourier transform) diffraction patterns were generated using the Gatan Digital Micrograph Program. The ^1H nuclear magnetic resonance (NMR) spectra were recorded using a Bruker AVANCE 400 MHz spectrometer equipped with 5 mm broadband probe head. The samples were dissolved in D_2O and measured at 25 °C. These 1-D measurements were recorded at with 8000 data points and repetition delay of 2 s. The spectra were processed using Topsin 3.2 software. Pt NC reduction kinetics was monitored on a Beckman–Coulter DU 800 spectrophotometer collected between 200 and 400 nm. The reaction was carried out in a quartz cell (1 cm path length) with K_2PtCl_4 (0.1 mM) as the precursor, $NaBH_4$ (0.1 mM) as the reducing agent, and peptides (0.1 mg/mL) as the surfactant.

Nitrobenzene Hydrogenation. Pd NCs were washed repeatedly with ethanol before catalytic reaction. The concentration of catalysts was determined by the inductively coupled plasma atomic emission spectroscopy (TJA RADIAL IRIS 1000 ICP-AES). The reaction was carried out at room temperature. The reaction time was 3.5 h. In a typical catalytic reaction, nitrobenzene (1.2 mmol), Pd catalysts suspension in ethanol (7.5 mM, 1.0 mL) and ethanol (9.0 mL) were mixed together and placed into a glass pressure vessel. In order to remove the air from the reaction system, the vessel was purged with H_2 before the catalytic reaction. Then, the vessel was pressurized with 1 bar. During the catalytic experiment, the pressure of H_2 was maintained constant. The intermediate catalytic products produced at different reaction time were analyzed by GC–MS (Shimadzu QP 2010 Plus). The calculation of the turnover frequency (TOF) is described in the Supporting Information.

Simulation. Adsorption energies and configurations of peptides TLHV, TLGV, and SSY on single-crystal seed *vs* single twinned seed were computed by molecular dynamic simulation using the CHARMM-METAL force field, the Nanoscale Molecular Dynamics program (NAMD), Hyperchem, and Materials Studio.[41] Simulation details are provided in the Supporting Information. All trajectories and identified representative conformations of the peptides on the surfaces and individual epitaxial contacts that contributed significantly to the adsorption energy were visually analyzed. Consensus adsorption energies were calculated, and uncertainties were determined using block averages across multiple trajectories (typically $< \pm 1$ kcal/mol).

Conflict of Interest: The authors declare no competing financial interest.

Acknowledgment. L. Ruan, Y. Li, and Y. Huang acknowledge support from the Office of Naval Research (ONR) (Award N00014-08-1-0985), the Army Research Office (ARO) (Award 54709- MS-PCS) and the Sloan Research Fellowship. X.D. acknowledges the support from the U.S. Department of Energy, Office of Basic Energy Sciences, Division of Materials Science and Engineering through Award DE-SC0008055. L. Ruan, C. Lee, X. Duan, and Y. Huang also acknowledge the Electron Imaging Center of Nanomachines for TEM and HRTEM support and UCLA Molecular Instrumentation Center for NMR and mass spectroscopy support. H. Ramezani-Dakhel and H. Heinz acknowledge support from the National Science Foundation (Award DMR 0955071), the Air Force Research Laboratory (AFRL and UES, Inc.), and the University of Akron. H. Ramezani-Dakhel and H. Heinz also acknowledge the allocation of computing resources at the Ohio Supercomputing Center.

Supporting Information Available: List of BP7A variants; additional TEM and HRTEM characterizations; circular dichroism

(CD) spectra; NMR spectra, ESI-MS spectra, UV−vis spectra; RMSD measurement in simulation; catalysis studies; and additional experimental and simulation details. This material is available free of charge *via* the Internet at http://pubs.acs.org.

REFERENCES AND NOTES

1. Buck, M. R.; Bondi, J. F.; Schaak, R. E. A Total-Synthesis Framework for the Construction of High-Order Colloidal Hybrid Nanoparticles. *Nat. Chem.* **2012**, *4*, 37–44.
2. Lohse, S. E.; Murphy, C. J. Applications of Colloidal Inorganic Nanoparticles: from Medicine to Energy. *J. Am. Chem. Soc.* **2012**, *134*, 15607–15620.
3. Zhou, K. B.; Li, Y. D. Catalysis Based on Nanocrystals with Well-Defined Facets. *Angew. Chem., Int. Ed.* **2012**, *51*, 602–613.
4. Lu, G.; Li, H.; Zhang, H. Gold Nanoparticle-Embedded PDMS Elastomers for Highly Sensitive Raman Detection. *Small* **2012**, *8*, 1336–1340.
5. Chen, H. J.; Shao, L.; Li, Q.; Wang, J. F. Gold Nanorods and Their Plasmonic Properties. *Chem. Soc. Rev.* **2013**, *42*, 2679–2724.
6. Macfarlane, R. J.; Lee, B.; Jones, M. R.; Harris, N.; Schatz, G. C.; Mirkin, C. A. Nanoparticle Superlattice Engineering with DNA. *Science* **2011**, *334*, 204–208.
7. Ye, X. C.; Chen, J.; Engel, M.; Millan, J. A.; Li, W. B.; Qi, L.; Xing, G. Z.; Collins, J. E.; Kagan, C. R.; Li, J.; *et al.* Competition of Shape and Interaction Patchiness for Self-Assembling Nanoplates. *Nat. Chem.* **2013**, *5*, 466–473.
8. Xia, Y. N.; Xiong, Y. J.; Lim, B.; Skrabalak, S. E. Shape-Controlled Synthesis of Metal Nanocrystals: Simple Chemistry Meets Complex Physics? *Angew. Chem., Int. Ed.* **2009**, *48*, 60–103.
9. Tao, A. R.; Habas, S.; Yang, P. D. Shape Control of Colloidal Metal Nanocrystals. *Small* **2008**, *4*, 310–325.
10. Huang, M. H.; Lin, P. H. Shape-Controlled Synthesis of Polyhedral Nanocrystals and Their Facet-Dependent Properties. *Adv. Funct. Mater.* **2012**, *22*, 14–24.
11. Elechiguerra, J. L.; Reyes-Gasga, J.; Yacaman, M. J. The Role of Twinning in Shape Evolution of Anisotropic Noble Metal Nanostructures. *J. Mater. Chem.* **2006**, *16*, 3906–3919.
12. Wiley, B.; Sun, Y. G.; Xia, Y. N. Synthesis of Silver Nanostructures with Controlled Shapes and Properties. *Acc. Chem. Res.* **2007**, *40*, 1067–1076.
13. Xiong, Y. J.; Xia, Y. N. Shape-Controlled Synthesis of Metal Nanostructures: the Case of Palladium. *Adv. Mater.* **2007**, *19*, 3385–3391.
14. Wu, J. B.; Qi, L.; You, H. J.; Gross, A.; Li, J.; Yang, H. Icosahedral Platinum Alloy Nanocrystals with Enhanced Electrocatalytic Activities. *J. Am. Chem. Soc.* **2012**, *134*, 11880–11883.
15. Langille, M. R.; Zhang, J.; Personick, M. L.; Li, S. Y.; Mirkin, C. A. Stepwise Evolution of Spherical Seeds into 20-Fold Twinned Icosahedra. *Science* **2012**, *337*, 954–957.
16. Zhang, H.; Xia, X. H.; Li, W. Y.; Zeng, J.; Dai, Y. Q.; Yang, D. R.; Xia, Y. N. Facile Synthesis of Five-Fold Twinned, Starfish-Like Rhodium Nanocrystals by Eliminating Oxidative Etching with a Chloride-Free Precursor. *Angew. Chem., Int. Ed.* **2010**, *49*, 5296–5300.
17. Dai, Z. R.; Sun, S. H.; Wang, Z. L. Shapes, Multiple Twins and Surface Structures of Monodisperse FePt Magnetic Nanocrystals. *Surf. Sci.* **2002**, *505*, 325–335.
18. Jiang, L.; Tang, Y. X.; Liow, C. H.; Wu, J. S.; Sun, Y. H.; Jiang, Y. Y.; Dong, Z. L.; Li, S. Z.; Dravid, V. P.; Chen, X. D. Synthesis of Fivefold Stellate Polyhedral Gold Nanoparticles with {110}-Facets *via* a Seed-Mediated Growth Method. *Small* **2013**, *9*, 705–710.
19. Wang, Y. M.; Chen, M. W.; Zhou, F. H.; Ma, E. High Tensile Ductility in a Nanostructured Metal. *Nature* **2002**, *419*, 912–915.
20. Chen, K. C.; Wu, W. W.; Liao, C. N.; Chen, L. J.; Tu, K. N. Observation of Atomic Diffusion at Twin-Modified Grain Boundaries in Copper. *Science* **2008**, *321*, 1066–1069.
21. Busse, C.; Polop, C.; Muller, M.; Albe, K.; Linke, U.; Michely, T. Stacking-Fault Nucleation on Ir(111). *Phys. Rev. Lett.* **2003**, *91*, 056103.
22. Algra, R. E.; Verheijen, M. A.; Borgstrom, M. T.; Feiner, L. F.; Immink, G.; van Enckevort, W. J. P.; Vlieg, E.; Bakkers, E. P. A. M. Twinning Superlattices in Indium Phosphide Nanowires. *Nature* **2008**, *456*, 369–372.
23. Chen, C. C.; Zhu, C.; White, E. R.; Chiu, C. Y.; Scott, M. C.; Regan, B. C.; Marks, L. D.; Huang, Y.; Miao, J. W. Three-Dimensional Imaging of Dislocations in a Nanoparticle at Atomic Resolution. *Nature* **2013**, *496*, 74–77.
24. Li, D. S.; Nielsen, M. H.; Lee, J. R. I.; Frandsen, C.; Banfield, J. F.; De Yoreo, J. J. Direction-Specific Interactions Control Crystal Growth by Oriented Attachment. *Science* **2012**, *336*, 1014–1018.
25. Liao, H. G.; Shao, Y.; Wang, C.; Lin, Y.; Jiang, Y. X.; Sun, S. G. TEM Study of Fivefold Twined Gold Nanocrystal Formation Mechanism. *Mater. Lett.* **2014**, *116*, 299–303.
26. Ringe, E.; Duyne, R. P. V.; Marks, L. D. Kinetic and Thermodynamic Modified Wulff Constructions for Twinned Nanoparticles. *J. Phys. Chem. C* **2013**, *117*, 15859–15870.
27. Zheng, H. M.; Smith, R. K.; Jun, Y. W.; Kisielowski, C.; Dahmen, U.; Alivisatos, A. P. Observation of Single Colloidal Platinum Nanocrystal Growth Trajectories. *Science* **2009**, *324*, 1309–1312.
28. Yuk, J. M.; Park, J.; Ercius, P.; Kim, K.; Hellebusch, D. J.; Crommie, M. F.; Lee, J. Y.; Zettl, A.; Alivisatos, A. P. High-Resolution EM of Colloidal Nanocrystal Growth Using Graphene Liquid Cells. *Science* **2012**, *336*, 61–64.
29. Dickerson, M. B.; Sandhage, K. H.; Naik, R. R. Protein- and Peptide-Directed Syntheses of Inorganic Materials. *Chem. Rev.* **2008**, *108*, 4935–4978.
30. Chiu, C. Y.; Ruan, L. Y.; Huang, Y. Biomolecular Specificity Controlled Nanomaterial Synthesis. *Chem. Soc. Rev.* **2013**, *42*, 2512–2527.
31. Ruan, L. Y.; Chiu, C. Y.; Li, Y. J.; Huang, Y. Synthesis of Platinum Single-Twinned Right Bipyramid and {111}-Bipyramid through Targeted Control over Both Nucleation and Growth Using Specific Peptides. *Nano Lett.* **2011**, *11*, 3040–3046.
32. Chiu, C. Y.; Li, Y. J.; Ruan, L. Y.; Ye, X. C.; Murray, C. B.; Huang, Y. Platinum Nanocrystals Selectively Shaped Using Facet-Specific Peptide Sequences. *Nat. Chem.* **2011**, *3*, 393–399.
33. Coppage, R.; Slocik, J. M.; Ramezani-Dakhel, H.; Bedford, N. M.; Heinz, H.; Naik, R. R.; Knecht, M. R. Exploiting Localized Surface Binding Effects to Enhance the Catalytic Reactivity of Peptide-Capped Nanoparticles. *J. Am. Chem. Soc.* **2013**, *135*, 11048–11054.
34. Patwardhan, S. V.; Patwardhan, G.; Perry, C. C. Interactions of Biomolecules with Inorganic Materials: Principles, Applications and Future Prospects. *J. Mater. Chem.* **2007**, *17*, 2875–2884.
35. Ruan, L. Y.; Ramezani-Dakhel, H.; Chiu, C. Y.; Zhu, E. B.; Li, Y. J.; Heinz, H.; Huang, Y. Tailoring Molecular Specificity Toward a Crystal Facet: a Lesson From Biorecognition Toward Pt {111}. *Nano Lett.* **2013**, *13*, 840–846.
36. Rothenstein, D.; Claasen, B.; Omiecienski, B.; Lammel, P.; Bill, J. Isolation of ZnO-Binding 12-Mer Peptides and Determination of Their Binding Epitopes by NMR Spectroscopy. *J. Am. Chem. Soc.* **2012**, *134*, 12547–12556.
37. Mirau, P. A.; Naik, R. R.; Gehring, P. Structure of Peptides on Metal Oxide Surfaces Probed by NMR. *J. Am. Chem. Soc.* **2011**, *133*, 18243–18248.
38. Ruan, L.; Zhu, E.; Chen, Y.; Lin, Z.; Huang, X.; Duan, X.; Huang, Y. Biomimetic Synthesis of an Ultrathin Platinum Nanowire Network with a High Twin Density for Enhanced Electrocatalytic Activity and Durability. *Angew. Chem., Int. Ed.* **2013**, *52*, 12577–12581.
39. Maksimuk, S.; Teng, X. W.; Yang, H. Planar Tripods of Platinum: Formation and Self-Assembly. *Phys. Chem. Chem. Phys.* **2006**, *8*, 4660–4663.
40. Li, Y. J.; Whyburn, G. P.; Huang, Y. Specific Peptide Regulated Synthesis of Ultrasmall Platinum Nanocrystals. *J. Am. Chem. Soc.* **2009**, *131*, 15998–15999.
41. Heinz, H.; Vaia, R. A.; Farmer, B. L.; Naik, R. R. Accurate Simulation of Surfaces and Interfaces of Face-Centered Cubic Metals Using 12−6 and 9−6 Lennard-Jones Potentials. *J. Phys. Chem. C* **2008**, *112*, 17281–17290.

42. Peelle, B. R.; Krauland, E. M.; Wittrup, K. D.; Belcher, A. M. Design Criteria for Engineering Inorganic Material-Specific Peptides. *Langmuir* **2005**, *21*, 6929–6933.
43. Hu, P. F.; Loo, J. A. Gas-Phase Coordination Properties of Zn^{2+}, Cu^{2+}, Ni^{2+}, and Co^{2+} with Histidine-Containing Peptides. *J. Am. Chem. Soc.* **1995**, *117*, 11314–11319.
44. Drochioiu, G.; Manea, M.; Dragusanu, M.; Murariu, M.; Dragan, E. S.; Petre, B. A.; Mezo, G.; Przybylski, M. Interaction of β-Amyloid(1−40) Peptide with Pairs of Metal Ions: an Electrospray Ion Trap Mass Spectrometric Model Study. *Biophys. Chem.* **2009**, *144*, 9–20.
45. Harada, M.; Kamigaito, Y. Nucleation and Aggregative Growth Process of Platinum Nanoparticles Studied by *In Situ* Quick XAFS Spectroscopy. *Langmuir* **2012**, *28*, 2415–2428.
46. Moddeman, W. E.; Morgan, K. A.; Jones, M. M.; Blackbur, Jr.; Albridge, R. G.; Kumar, G. Photoelectron Spectroscopy of Coordination Compounds. III. Comparison of Platinum(II) and Platinum(IV) Compounds. *Inorg. Chem.* **1972**, *11*, 1715–1717.
47. Timari, S.; Cerea, R.; Varnagy, K. J. Characterization of CuZnSOD Model Complexes from a Redox Point of View: Redox Properties of Copper(II) Complexes of Imidazole Containing Ligands. *Inorg. Biochem.* **2011**, *105*, 1009–1017.
48. Henglein, A.; Giersig, M. Reduction of Pt(II) by H_2: Effects of Citrate and NaOH and Reaction Mechanism. *J. Phys. Chem. B* **2000**, *104*, 6767–6772.
49. Yao, T.; Liu, S. J.; Sun, Z. H.; Li, Y. Y.; He, S.; Cheng, H.; Xie, Y.; Liu, Q. H.; Jiang, Y.; Wu, Z. Y.; *et al.* Probing Nucleation Pathways for Morphological Manipulation of Platinum Nanocrystals. *J. Am. Chem. Soc.* **2012**, *134*, 9410–9416.
50. Li, Y. J.; Huang, Y. Morphology-Controlled Synthesis of Pt Nanoparticles with Specific Peptides. *Adv. Mater.* **2010**, *22*, 1921–1925.
51. Heinz, H.; Farmer, B. L.; Pandey, R. B.; Slocik, J. M.; Patnaik, S. S.; Pachter, R.; Naik, R. R. Nature of Molecular Interactions of Peptides with Gold, Palladium, and Pd−Au Bimetal Surfaces in Aqueous Solution. *J. Am. Chem. Soc.* **2009**, *131*, 9704–9714.
52. Feng, J.; Pandey, R. B.; Berry, R. J.; Farmer, B. L.; Naik, R. R.; Heinz, H. Adsorption Mechanism of Single Amino Acid and Surfactant Molecules to Au {111} Surfaces in Aqueous Solution: Design Rules for Metal-Binding Molecules. *Soft Matter* **2011**, *7*, 2113–2120.
53. Heinz, H.; Lin, T. J.; Mishra, R. K.; Emami, F. S. Thermodynamically Consistent Force Fields and Molecular Models for the Assembly of Inorganic, Organic, and Biological Hybrid Nanostructures: the Interface Force Field. *Langmuir* **2013**, *29*, 1754–1765.
54. Ramezani-Dakhel, H.; Mirau, P. A.; Naik, R. R.; Knecht, M. R.; Heinz, H. Stability, Surface Features, and Atom Leaching of Palladium Nanoparticles: Toward Prediction of Catalytic Functionality. *Phys. Chem. Chem. Phys.* **2013**, *15*, 5488–5492.
55. Zhang, H.; Li, W. Y.; Jin, M. S.; Zeng, J. E.; Yu, T. K.; Yang, D. R.; Xia, Y. N. Controlling the Morphology of Rhodium Nanocrystals by Manipulating the Growth Kinetics with a Syringe Pump. *Nano Lett.* **2011**, *11*, 898–903.
56. Chiu, C. Y.; Wu, H.; Yao, Z.; Zhou, F.; Zhang, H.; Ozolins, V.; Huang, Y. Facet-Selective Adsorption on Noble Metal Crystals Guided by Electrostatic Potential Surfaces of Aromatic Molecules. *J. Am. Chem. Soc.* **2013**, *135*, 15489–15500.
57. Huang, X. Q.; Li, Y. J.; Li, Y. J.; Zhou, H. L.; Duan, X. F.; Huang, Y. Synthesis of PtPd Bimetal Nanocrystals with Controllable Shape, Composition, and Their Tunable Catalytic Properties. *Nano Lett.* **2012**, *12*, 4265–4270.
58. Li, C. C.; Sato, R.; Kanehara, M.; Zeng, H. B.; Bando, Y.; Teranishi, T. Controllable Polyol Synthesis of Uniform Palladium Icosahedra: Effect of Twinned Structure on Deformation of Crystalline Lattices. *Angew. Chem., Int. Ed.* **2009**, *48*, 6883–6887.
59. Calvo, F.; Carre, A. Structural Transitions and Stabilization of Palladium Nanoparticles Upon Hydrogenation. *Nanotechnology* **2006**, *17*, 1292–1299.